RESEARCH PAPER

PCCP
www.rsc.org/pccp

Low-temperature and high-pressure induced swelling of a hydrophobic polymer-chain in aqueous solution

Dietmar Paschek,* Sascha Nonn and Alfons Geiger

Physikalische Chemie, Universität Dortmund, Otto-Hahn-Str. 6, D-44221 Dortmund, Germany. E-mail: dietmar.paschek@udo.edu

Received 4th May 2005, Accepted 8th June 2005
First published as an Advance Article on the web 20th June 2005

We report molecular dynamics simulations of a hydrophobic polymer-chain in aqueous solution between 260 K and 420 K at pressures of 1 bar, 3000 bar, and 4500 bar. The simulations reveal a hydrophobically collapsed structure at low pressures and high temperatures. At 3000 bar and about 260 K and at 4500 bar and about 260 K, however, an abrupt transition to a swelled state is observed. The transition is driven by a smaller volume and a remarkably strong lower enthalpy of the swelled state, indicating a steep positive slope of the corresponding transition line. The swelling is strongly stabilized by the energetically favorable state of water in the polymer's hydrophobic first hydration shell at low temperatures. This finding is consistent with the observation of a positive heat capacity of hydrophobic solvation. Moreover, the slope and location of the estimated swelling transition line for the collapsed hydrophobic chain coincides remarkably well with the cold denaturation transition of proteins.

1. Introduction

Hydrophobic effects have been shown to be of relevance for a wide range of physicochemical and biophysical phenomena.[1–3] In particular, hydrophobic interaction is seen as an important driving force in the process of folding proteins.[4–6] Consequently, a wealth of studies on hydrophobic interactions using molecular simulation techniques have been undertaken over the past three decades.[7–29] Simulation studies have revealed that the contact state of a pair of hydrophobic particles in aqueous solution is entropically stabilized at ambient conditions.[10,11] In addition, the role of the solvation heat capacity has been investigated recently.[21–28] In general, the dissolution of hydrophobic particles is accompanied by an increase of the heat capacity.[30–32] As a consequence, the dissolution of a hydrophobic particle is found to be increasingly enthalpically stabilized with decreasing temperature.[28]

Biopolymers such as proteins remain stable and functional only in a limited pressure and temperature range.[33–35] Increasing temperatures lead to structures distinct from the native folded state. This is often accompanied by large fluctuations and aggregation phenomena. Hence, pressure effects on proteins are of interest in biotechnology and biology,[36] as pressure is shifting the equilibrium of protein conformations without increasing thermal fluctuations.[37–40] Proteins undergo unfolding upon application of pressures above 2 kbar. High pressures are also able to dissociate protein complexes.[41,42] The solvent water plays a crucial role in the effect of pressure in protein unfolding[35,38,43,44] and the addition of co-solvents is found to have a significant influence on the size, location and shape of the stability region of proteins.[45,46]

At high pressures (>2 kbar), the volume of hydrated proteins decreases upon unfolding. This seemed to be inconsistent with the assumption of protein unfolding being equivalent to the transfer of hydrophobic groups from the protein interior to the aqueous solvent, since the volume change upon transfer of hydrophobic groups to water are positive. Hummer *et al.*[47] suggested a scenario in which pressure unfolding of proteins is modeled as the transfer of water into the protein hydrophobic core with increasing pressure. This transfer of water molecules into the protein interior is essential for the pressure unfolding process, leading to the dissociation of close hydrophobic contacts and subsequent swelling of the hydrophobic protein interior through insertions of water molecules.[47] The characteristic features of water-mediated interactions between hydrophobic solutes in water are found to be pressure-dependent. In particular, with increasing pressure the solvent-separated configurations in the solute–solute potential of mean force is stabilized with respect to the contact configurations. In addition, the desolvation barrier between contact and solvent-separated configurations increases monotonically with P. The locations of the minima and the barrier move toward shorter separations, and pressure effects are considerably amplified for larger hydrophobic solutes.[18–20]

Pressure also changes the entropy/enthalpy balance of the hydrophobic interactions. Ghosh *et al.* found that the contact minimum is dominated by entropy, whereas the solvent-separated minimum is stabilized by a favorable enthalpy of association.[18,19] Both the entropy and enthalpy at the contact minimum seem to change little with increasing pressure, leading to the relative pressure insensitivity of the contact minimum configurations. In contrast, the solvent-separated configurations are increasingly stabilized at higher pressures by enthalpic contributions that prevail over the slightly unfavorable entropic contributions to the free energy.[19]

In this contribution, we focus particularly on the scenario proposed by Hummer *et al.*[47] of water penetrating into the protein interior at elevated pressures. Here we study a simplistic model system of a protein: A fully hydrated polymer-chain, consisting of 20 interconnected hydrophobic spheres. The polymer-chain approach has been recently advocated by Chandler and co-workers,[48–50] suggesting that the collapse of a hydrophobic polymer chain is driven by what they call a drying transition. In ref. 49 the hydrophobic chain is modeled by repulsive polymer/water interactions only, whereas the solvent is represented by a coarse grained model. In the recent work of Ghosh *et al.*,[51] molecular dynamics simulations of a polymer-chain in an explicit solvent reveal the effect of dissolved salts on the polymer configuration, increasingly favoring compact folded configurations of the polymer with increasing salt concentration. In the above mentioned studies a "stiff" polymer chain was employed, which exhibits a

DOI: 10.1039/b506207a

stretched equilibrium configuration in absence of a solvent. Thus the energy needed to bend the polymer-chain is used to counterbalance the tendency to minimize the solvent accessible surface. In the present study no such terms are employed, hence a chain of linked hydrophobic particles, free of bond-angles and dihedral potential barriers is considered. Thus the reported configurational changes of the polymer have to be completely attributed to the influence of the solvent.

2. Computational methods

2.1. MD Simulation details

We report molecular dynamics (MD) simulations of a purely hydrophobic polymer-chain dissolved in an aqueous solution. The polymer-chain consists of 20 hydrophobic polymer beads, represented by Lennard-Jones interaction sites X with $\sigma_{XX} = 3.975$ Å, $\varepsilon_{XX}k_B^{-1} = 214.7$ K.[27] The water–polymer cross parameters were obtained using the conventional Lorentz–Berthelot mixing rules with $\sigma_{ij} = (\sigma_{ii} + \sigma_{jj})/2$ and $\varepsilon_{ij} = \sqrt{\varepsilon_{ii}\varepsilon_{jj}}$. The polymer sites are linked by rigid bonds of 4.2 Å length. This bond-length was determined to represent the bead–bead contact distance for non-linked particles in aqueous solution.[28] In addition, this value corresponds roughly to the distance between adjacent hydrophobic Valine sidechains in a polypeptide. All intramolecular non-bonded interactions were taken into account, except interactions between adjacent bonded sites. No additional bond-bending or torsional potentials were used. The water phase is represented by 1000 TIP5P water molecules.[52] The TIP5P model was chosen, since it represents the hydrophobic solvation behavior of water on the low-temperature side probably most realistically among the simple point charge models.[27] Moreover, the temperature dependent strength of the hydrophobic interaction was found to be quite critically linked to the temperature dependence of the water expansivity.[27] The simulations discussed here were carried over a broad temperature range at pressures of 1 bar, 3000 bar, and 4500 bar. Individual MD-simulations extend up to 100 ns, while the total simulation time adds up to about 0.76 μs. A simulation protocol is given in Table 1.

The MD-simulations are carried out in the NPT ensemble using the Nosé–Hoover thermostat[53,54] and the Rahman–Parrinello barostat[55,56] with coupling times $\tau_T = 1.5$ ps and $\tau_p = 2.5$ ps (assuming an isothermal compressibility of $\chi_T = 4.5 \times 10^{-5}$ bar^{-1}), respectively. The electrostatic interactions are treated in the "full potential" approach by the smooth particle mesh Ewald summation[57] with a real space cutoff of 0.9 nm and a mesh spacing of approximately 0.12 nm and 4th order interpolation. The Ewald convergence factor α was set to 3.38 nm^{-1} (corresponding to a relative accuracy of the Ewald sum of 10^{-5}). A 2.0 fs timestep was used for all simulations. Solvent constraints were solved using the SETTLE procedure,[58] while the SHAKE-algorithm was used for the polymer constraints.[59] For all simulations reported here the GROMACS 3.2 program[60,61] was used. Statistical errors in the analysis were computed using the method of Flyvbjerg and Petersen.[62] For each system an initial equilibration run of about 1 ns length was performed using the Berendsen weak coupling scheme for pressure and temperature control ($\tau_T = \tau_p = 0.5$ ps).[63]

It should be mentioned that the completely stretched polymer extends to about 8 nm, which exceeds the used box length about 2.5 times. However, in practice, contacts between the polymer and its virtual image were not observed during the simulation runs discussed here.

Table 1 Simulation protocol for the performed MD-simulations. τ: Simulation time; $\langle V\rangle$: Average box-volume; $\langle E\rangle$: Average total energy

T/K	τ/ns	$\langle V\rangle$/nm^3	$\langle E\rangle$/kJ mol^{-1}
		1 bar:	
260	80	31.803 ± 0.006	−38 065 ± 6
280	54	31.710 ± 0.002	−35 036 ± 5
300	30	32.008 ± 0.003	−32 469 ± 6
320	30	32.563 ± 0.003	−30 128 ± 4
340	30	33.324 ± 0.003	−27 936 ± 5
380	27	35.450 ± 0.020	−23 799 ± 20
420	28	38.880 ± 0.050	−19 772 ± 30
		3000 bar:	
260	100	27.868 ± 0.003	−37 432 ± 9
280	100	28.043 ± 0.002	−35 138 ± 3
300	50	28.305 ± 0.002	−33 067 ± 3
360	30	29.428 ± 0.002	−27 535 ± 2
400	30	30.384 ± 0.001	−24 252 ± 3
		4500 bar:	
280	73	26.935 ± 0.002	−35 222 ± 3
300	73	27.212 ± 0.001	−33 220 ± 3
320	25	27.514 ± 0.002	−31 360 ± 3
360	25	28.206 ± 0.001	−27 918 ± 3

2.2. Energy analysis

In order to assign potential energies to individual molecules and thus to be able to distinguish between contributions from the "hydration shell" and from the "bulk" we determine energies by a reaction field method based on the minimum image cube. This "cubic" cutoff procedure was originally proposed by Neumann.[64] Roberts and Schnitker[65,66] have shown that the obtained energy estimates compare very well with the Ewald-summation including tin-foil boundary conditions.

For convenience, we divide the total potential energies E in contributions assigned to the individual molecules with

$$E = \sum_{i=1}^{M} E_i$$
$$E_i = \left(\frac{1}{2}\sum_{j=1}^{M} E_{ij}\right) + E_{i,\mathrm{corr.}}, \qquad (1)$$

where E_i is the potential energy assigned to molecule i, M is the total number of molecules. The molecule–molecule pair energy

$$E_{ij} = \sum_{\alpha}\sum_{\beta}\left\{4\varepsilon_{i\alpha j\beta}\left[\left(\frac{\sigma_{i\alpha j\beta}}{r_{i\alpha j\beta}}\right)^{12} - \left(\frac{\sigma_{i\alpha j\beta}}{r_{i\alpha j\beta}}\right)^{6}\right] + \frac{1}{4\pi\varepsilon_0}\frac{q_{i\alpha}q_{j\beta}}{r_{i\alpha j\beta}}\right\} \qquad (2)$$

is then obtained as the sum over discrete interaction sites α and β, with $r_{i\alpha j\beta} = |\vec{r}_{j\beta} - \vec{r}_{i\alpha}|$ based on the molecule/molecule center of mass minimum image separation. We employ long range corrections $E_{i,\mathrm{corr.}} = E_{i,\mathrm{corr.}}^{\mathrm{el}} + E_{i,\mathrm{corr.}}^{\mathrm{LJ}}$ accounting for electrostatic, as well as Lennard Jones interactions. The electrostatic correction[65,66]

$$E_{i,\mathrm{corr.}}^{\mathrm{el}} = \frac{1}{4\pi\varepsilon_0}\frac{2\pi}{3V}\vec{D}\,\vec{d}_i \qquad (3)$$

is a reaction field term, corresponding to the cubic cutoff, assuming an infinitely large dielectric constant. Here $\vec{d}_i = \sum_\alpha q_{i\alpha}\vec{r}_{i\alpha}$ is the dipole moment of molecule i, $\vec{D} = \sum_i \vec{d}_i$ is the total dipole moment of all molecules in the cubic simulation box and V is the instantaneous volume of the simulation box. Finally, also the long range Lennard-Jones corrections for the minimum image were taken into account, as outlined in ref. 28.

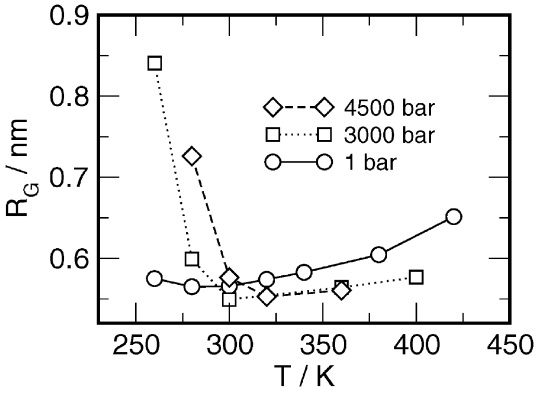

Fig. 1 Average radius of gyration R_G of the hydrated polymer as obtained for all temperatures at 1 bar, 3000 bar and 4500 bar. The lines are drawn to guide the eye.

3. Results

The structure of the dissolved hydrophobic polymer-chain is characterized by its radius of gyration $R_G^2 = 1/20\sum_{i=1}^{20}(\vec{r}_i - \vec{c})^2$ with $\vec{c} = 1/20\sum_{i=1}^{20}\vec{r}_i$. The typical conformation of this polymer at high temperatures and low pressures is a compact, collapsed state with an average R_G between 0.5 nm and 0.6 nm, as shown in Fig. 1. A snapshot of a representative collapsed-chain configuration is shown in Fig. 2. The conformational distribution with respect to R_G is found to be narrow, with a half width at half maximum of R_G of about 0.1 nm. Test-simulations at 300 K and ambient pressure conditions, starting with a swelled configuration of $R_G \approx 1$ nm, show a collapse on a timescale <1 ns. The polymer/water center of mass pair correlation functions (given in Fig. 3) reveal that in the collapsed state water is completely excluded from the polymer interior.

The temperature dependence of the average radius of gyration at a pressure of 1 bar is characterized by a shallow minimum at about 300 K (Fig. 1). With increasing temperature the distribution of R_G more or less maintains its shape, but is becoming broader with its maximum shifting to larger values as shown in Fig. 4. The high-temperature behavior is more or less similar for all pressures discussed here. In addition, a slight penetration of water into the polymer interior is observed at 420 K (see Fig. 3).

At lower temperatures, however, a different behavior is starting to emerge. From the time evolution of R_G, shown in Fig. 4 it is evident that at about 260 K and 1 bar the polymer increasingly starts to explore extended-chain configurations. These extended-chain states are occurring only rather infrequently and are short-lived with a life-time of about 1 ns. We would like to emphasize that the 280 K/3000 bar and 300 K/4500 bar trajectories show a similar behavior. Again, the extended-chain configurations are rather short-lived with the chain quickly returning to the collapsed state. Quantitatively, compared to the 260 K/1 bar simulation, an increase of the population of swelled states is found, which is due to the apparent higher frequency of large amplitude R_G-fluctuations. The most striking difference, however, is observed for 260 K at 3000 bar and 280 K at 4500 bar. Here the extended-chain configurations are dominating, although an equilibrium between collapsed and swelled states is still maintained. The radius of gyration is showing an apparently bimodal distribution at 260 K at 3000 bar and a broad distribution at 280 K at 4500 bar. The representation of both (swelled and compact) at each of these states, strongly suggests that the corresponding conformational transition temperatures are located in close proximity to these temperatures.

The temperature dependence of the average R_G at different pressures, as given in Fig. 1, suggests that the high-temperature collapsed-chain state is more compact at elevated pressures, which would correspond to a more compressed coiled state. At 280 K and 3000 bar and 300 K and 4500 bar, however, the situation has already started changing, and the tendency to explore more extended configurations leads to an increase in R_G which is quickly progressing upon cooling. The low temperature destabilization of the collapsed state is in line with the decreased stability of hydrophobic contacts observed for elevated pressures.[19,20,47]. Fig. 1 implies that the transition towards a swelled state at 3000 bar and 4500 bar occurs in a rather narrow temperature interval, suggesting a rather large enthalpy difference between collapsed and swelled states. In other words: it shows a large "cooperativity". Thermodynamical consistency requires that the swelled low temperature state has to be energetically more stable than the compact state and that it has to occupy a smaller total volume. Fig. 5 shows a comparison of the time-evolution of the total potential energy

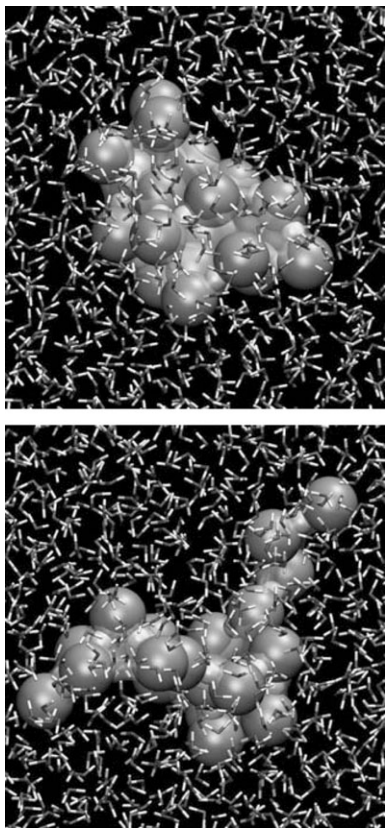

Fig. 2 Representative configurations of the hydrophobic polymer in aqueous solution as obtained from simulations at 3000 bar. Top: Collapsed configuration observed at 300 K. Bottom: Swelled configuration observed at 260 K.

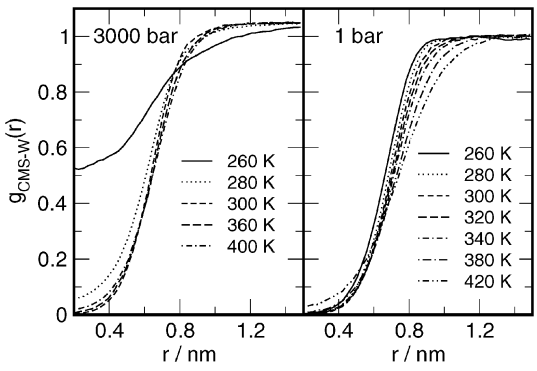

Fig. 3 Polymer/water center of mass pair correlation functions for several selected simulated state points.

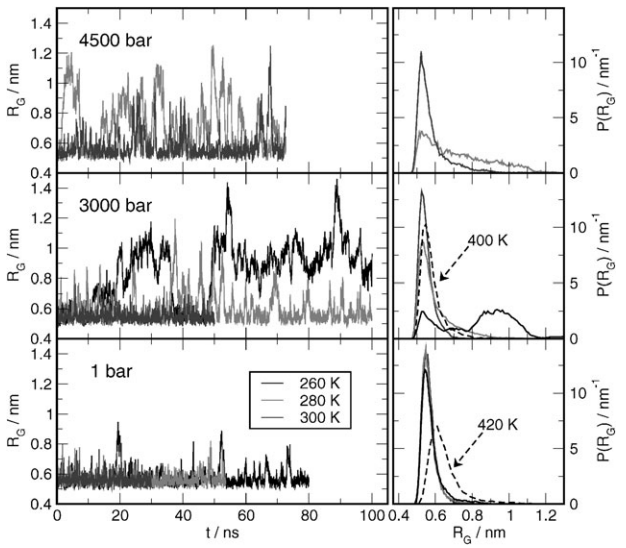

Fig. 4 Time-evolution and corresponding probability density distribution of the polymer's radius of gyration. Shown are the lowest temperatures at 1 bar (bottom), 3000 bar and 4500 bar (top). The dashed line indicates the probability distribution obtained for the highest temperatures, respectively.

E and box-volume V with R_G for 260 K at 3000 bar. In order to make the trends more clearly visible, the noise in the fluctuations has been reduced by Savitzky–Golay filtering.[67] Both, the potential energy as well as the box-volume are clearly anti-correlated with respect to R_G. The swelled state of the polymer is enthalpically stabilized with an energy difference of $\Delta E_u = E(\text{swell.}) - E(\text{coll.})$ of -182 kJ mol^{-1} at 3000 bar and of -82 kJ mol^{-1} at 4500 bar. The swelled state leads also to smaller box volumes, with $\Delta V_u = V(\text{swell.}) - V(\text{coll.})$ of -20 ml mol^{-1} at 3000 bar and of -10 ml mol^{-1}. We would like to point out the observed enthalpy and volume changes are of similar magnitude as observed for some proteins[34] and peptides.[68]

In the following paragraphs we would like to show that the energy and volume change can be attributed almost quantitatively to the first hydration shell of the polymer and have to be almost exclusively attributed to the solvent. Fig. 6 depicts the polymer-beads/water-oxygen site–site pair correlation functions for the collapsed and swelled states obtained at 260 K

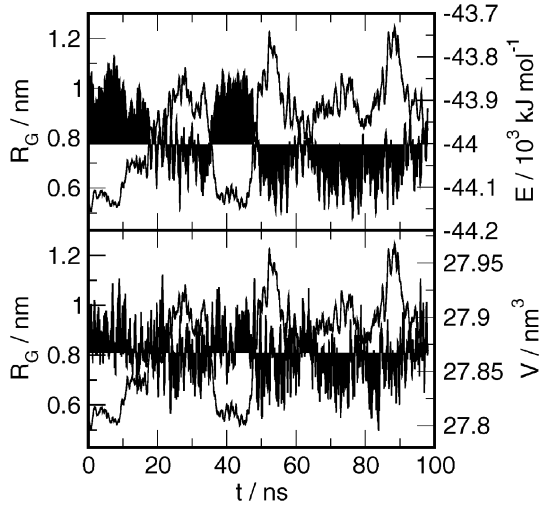

Fig. 5 Time evolution of the radius of gyration of the polymer (thin line), total potential energy (filled polygon to average value, top) and box volume (filled polygon to average value, bottom) as obtained from the simulation at 260 K and 3000 bar. Potential energies and box-volumes were directly taken from GROMACS simulation output. In order to reduce the noise, all data were smoothed using the same Savitzky–Golay filter.[67]

and 3000 bar. The first minimum, located at a distance of 0.52 nm, indicates the spatial dimension of the first hydration shell. The average number of water neighbors around each polymer site changes about 40% from 11.5 to 16 upon swelling. At 4500 bar a qualitatively similar behavior is observed. In order to quantify the changes in the hydration shell, we define the volume occupied by the polymer and the first hydration shell as the volume with a distance of $R \leq 0.52$ nm with respect to any polymer-site. The properties obtained for the hydration shell of the collapsed and swelled polymer and the water bulk are summarized in Table 2.

The polymer/water center of mass pair correlation function as well as the potential energy of water as a function of the distance to the polymer center for the collapsed and swelled states (see caption of Table 2 for the definition) are given in Fig. 7. From Fig. 7b it is evident that in the region of the polymer/water interface (at $r \approx 0.9$ nm) water is 0.3 kJ mol^{-1} more stable than in the bulk. However, due to the lack of water neighbors, a further penetration of individual waters into the collapsed hydrophobic coil is energetically unfavorable, as the steep increase in Fig. 7b indicates. When drawing the balance over all water molecules in the hydration shell, energy gains and penalties cancel out almost completely and the average potential energy of a water molecule in the hydration shell of the collapsed polymer is nearly identical to the value observed for the water bulk at 3000 bar and slightly higher (more unstable) at 4500 bar (see Table 2). For the case of the swelled polymer, the energy penalty is absent and the water in the hydration shell gains -0.78 kJ mol^{-1} potential energy per water molecule with respect to the bulk on average (-0.26 kJ mol^{-1} at 4500 bar). The potential energy difference about $\Delta E_u \approx [E(\text{shell,swell.}) - E(\text{bulk})]N(\text{shell,swell.}) - [E(\text{shell,coll.}) - E(\text{bulk})]N(\text{shell,coll.}) + E(\text{polymer,swell.}) - E(\text{polymer,coll.}) = -138$ kJ mol^{-1} (-60 kJ mol^{-1}) accounts largely for the observed total energy difference of about -182 kJ mol^{-1} (-82 kJ mol^{-1}). The potential energy of the polymer changes by just 8.4 kJ mol^{-1} (14.5 kJ mol^{-1}), which is due to the fact that the loss of intramolecular interactions when going from the collapsed to the swelled state is almost completely compensated by polymer/solvent interactions (The values for 4500 bar are given in parentheses). Hence the extended-chain configurations at low temperatures appear to be largely solvent-stabilized.

The volume change upon swelling is $\Delta V_{m,u} \approx [V_m(\text{shell, swell.}) - V_m(\text{bulk})]N(\text{shell,swell.}) - [V_m(\text{shell,coll.}) - V(\text{bulk})]N(\text{shell,coll.}) = -57$ ml mol^{-1} at 4500 bar and $\Delta V_{m,u} \approx -21$ ml mol^{-1} for the 4500 bar-isobar. The origin of the negative volume change upon swelling is indicated in Fig. 8. Here the free volume fraction accessible to a small sphere is shown as a function of distance to the polymer center. For the collapsed state, apparently an excess free volume in the polymer interior is available to a hard sphere particle which is

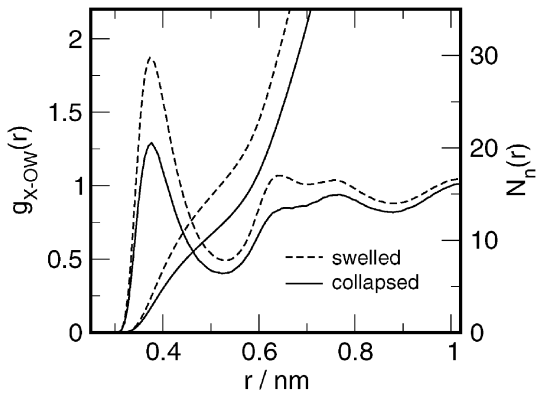

Fig. 6 Polymer–bead/water–oxygen site–site pair correlation function $g_{X\text{–}OW}(r)$ and integrated number of nearest neighbors $N_n(r)$ for the collapsed and swelled states at 260 K and 3000 bar.

Table 2 Energies and volumes obtained for the bulk and hydration shell for the given statepoints. The "hydration shell" is defined as the volume with a distance $R \leq 0.52$ nm to any polymer site, whereas the "bulk" is obtained for distances of $R > 1.0$ nm. V (Shell) denotes the corresponding volume occupied by the polymer and its first hydration shell. $N(H_2O)$ gives the average number of hydration shell water molecules. The hydration shell water molar volumes are according to $V_m(H_2O) = V(\text{Shell})/N(H_2O) * N_A$, where N_A is the Avogadro number. The potential energies E of the polymer and water in bulk and shell are given per molecule. "collapsed" and "swelled" states are defined by $R_G < 0.65$ nm and $R_G > 0.8$ nm, respectively

Bulk:	260 K; 3000 bar		280 K; 4500 bar	
$E(H_2O)$/kJ mol^{-1}	-43.657 ± 0.004		-42.081 ± 0.003	
$V_m(H_2O)$/cm^3 mol^{-1}	16.02 ± 0.05		15.50 ± 0.02	
Hydration shell:	"Collapsed"	"Swelled"	"Collapsed"	"Swelled"
$N(H_2O)$	126.5 ± 2.1	184.2 ± 2.8	129.4 ± 1.3	173.0 ± 2.0
V(Shell)/nm^3	4.51 ± 0.09	5.96 ± 0.08	4.49 ± 0.03	5.58 ± 0.07
$V_m(H_2O)$/cm^3 mol^{-1}	21.47 ± 0.05	19.49 ± 0.05	20.97 ± 0.07	19.46 ± 0.07
$E(H_2O)$/kJ mol^{-1}	-43.63 ± 0.05	-44.43 ± 0.03	-41.85 ± 0.02	-42.34 ± 0.03
E(Polymer)/kJ mol^{-1}	-149.7 ± 0.5	-141.3 ± 0.6	-141.2 ± 0.2	-126.7 ± 0.5

absent in the swelled state. The hydration shell around the hydrophobic chain appears to be more tightly packed, so that the average free volume fraction is even lower than for the bulk water. Hence the increase in solvent accessible surface (increasing number of hydration shell water molecules) is overcompensated by the decrease in molar volume of water in the swelled hydration shell state. The hydration shell volume of the collapsed state includes, of course, the volume of the hydrophobic core, which is made accessible to the solvent upon unfolding of the chain.

Finally, we would like to compare the behavior of the hydrophobic polymer with the experimentally obtained stability diagrams of proteins. Interpolating the R_G-data from Fig. 1 and assuming that the transition appears at $R_G \approx 0.7$ nm, we obtain $T_u \approx 268$ K and 282 K for 3000 bar and 4500 bar, respectively. Using the enthalpies $\Delta H_u \approx \Delta E_u + P\Delta V_u$ and volumes ΔV_u as derived above from data of Table 2, we obtain a slope of the coexistence line of $dp_{eq}/dT = \Delta H_U/T_u\Delta V_U$ of about 100 bar K^{-1} for both pressures, apparently consistent with the observed shift of the transition temperatures from 268 K to 282 K. Although having more data would be desirable, we might conjecture that the slope does not seem to change much, but the enthalpy and volume differences tend to decrease with increasing pressure. Since the differences might disappear completely at higher pressures, the swelling transition of the hydrophobic polymer probably ends up in an "upper critical point" (The term "critical point" has to be used with caution here since the swelling transition has a smooth and smeared out character due to the finite size of the polymer). In Fig. 9 the estimated swelling transition line, as well as the experimentally determined stability diagrams of two proteins (SNase[43] and Ubiquitin[44]) are shown. We would like to point out that the location and slope of the swelling transition shows remarkable similarity to the given cold-denaturation lines. The hydrophobic polymer apparently behaves as suggested by the water penetration scenario according to Hummer *et al.*[47] In the present case the energy stabilization of the swelled configuration is dominated by the energy gain of the hydration water. In a real polypeptide this is not necessarily true. Backbone hydration and the equilibrium between intra- and intermolecular hydrogen bonds will certainly play an important role. How this delicate balance might influence the equilibrium between swelled and collapsed configuration should be further investigated. The high temperature side of the protein stability diagram might not be accessible by our simple model since it is largely related to internal secondary structural transformation to a "molten globule" state.[69]

In the present simulation study the energy gain upon unfolding is apparently a consequence of the increasing water–water pair interactions in the hydration shell at low temperatures.[28] The hydrogen bond network in the hydration shell starts disintegrating upon heating more strongly than in the bulk since no hydrogen bonds can be formed to the hydrophobic Lennard-Jones particles.[28] The balance between strengthened hydrogen bonds and enhanced disintegration of the hydrogen bond network is widely regarded as the mechanism leading to the positive solvation heat capacity associated

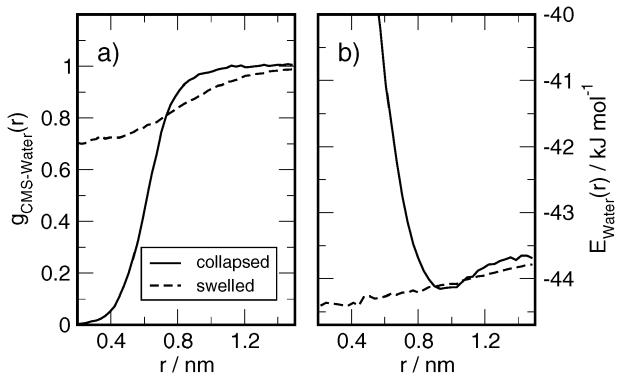

Fig. 7 (a) Polymer/water center of mass pair correlation function for the collapsed and swelled states at 260 K and 3000 bar. (b) Potential energy of the water molecules as a function of distance to the polymer center.

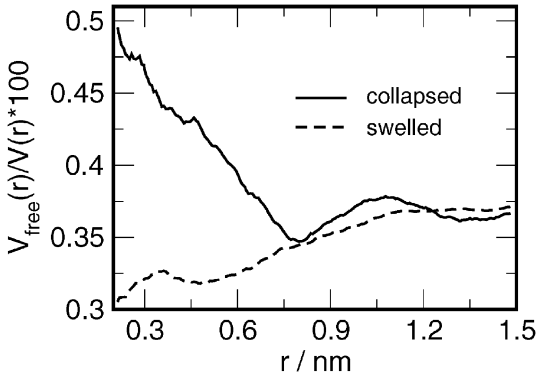

Fig. 8 Free volume fraction accessible to a small hard sphere particle as a function of distance to the polymer center. Given are dependencies for the collapsed and swelled states at 260 K and 3000 bar. The diameter of the particle with $\sigma_{Y\text{–}OW} = 2.5$ Å and $\sigma_{Y\text{–}X} = 2.93$ Å is scaling as the corresponding Lennard-Jones σ.

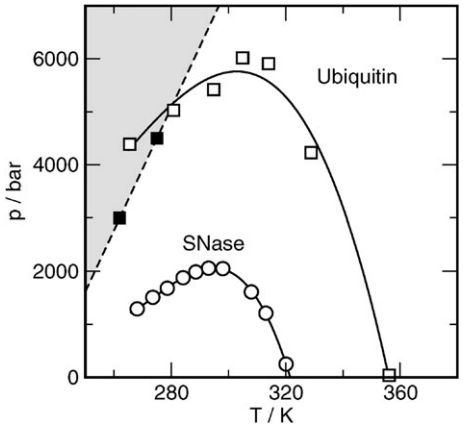

Fig. 9 Sketch of the swelling line of the hydrophobic polymer used in this study compared with experimental stability diagrams as obtained for SNase[43] and Ubiquitin.[44]

with hydrophobic hydration.[5,70] This mechanism underlying cold swelling is hence in line with the lattice model calculations proposing a cold swelling by De Los Rios *et al.*[71,72] In their calculation the different heat capacities in the solvent and hydration shell[71,72] are explicitly based on different hydrogen bond equilibria for both regions.[70,73] As a consequence, and according to our calculations, we expect the observed transition temperature to be critically linked by the change of the solvent heat capacity. Finally, we would like to point out that the pressure dependence of the low temperature swelling line of the hydrophobic polymer chain has some similarity with the behavior observed recently for a lattice model protein by Marqués *et al.*[74] However, their assumption of the inability of water to arrange energetically favourably around hydrophobic solutes at moderate pressures, hence limiting the cold denaturation window to the elevated pressure interval where a stable ice II phase exists, seems to be at odds with our findings and previous model calculations.[71,72]

4. Conclusion

Molecular dynamics simulations of a hydrophobic polymer-chain in aqueous solution between 260 K and 420 K at pressures of 1 bar, 3000 bar, and 4500 bar reveal a hydrophobically collapsed state at low pressures and high temperatures. At about 268 K and 3000 bar and at 282 K and 4500 bar a transition to a swelled state is observed. The transition is driven by a smaller volume and a remarkably strong lower enthalpy of the swelled state. The volume effect is basically due to a smaller net-volume of the extended hydrated state compared to the collapsed state, exhibiting pronounced hydrophobic cavity volumes and penetration of the internal volume by water. Moreover, the extended-chain structure is almost completely energetically stabilized by the lower potential energy of the water molecules in the hydration shell. Consequently, the increasingly stable water–water hydrogen bonds close to a hydrophobic particle, leading to the positive heat capacity of solvation, which is a signature for hydrophobic hydration,[70] is the key to the observed behavior. The strong energy and volume differences indicate a steep positive slope of the corresponding transition line of about 100 bar K^{-1}. The observed stability line for the collapsed hydrophobic chain shows strong similarity with the lower temperature side of the stability diagram of proteins in aqueous solution.

Acknowledgements

Financial support by the Deutsche Forschungsgemeinschaft (DFG-Forschergruppe 436) and University of Dortmund (Forschungsband ''Molekulare Aspekte der Biowissenschaften'') is gratefully acknowledged. We would like to thank Angel E. García for helpful remarks.

References

1 C. Tanford, *The Hydrophobic Effect: Formation of Micelles and Biological Membranes*, John Wiley & Sons, New York, 2nd edn., 1980.
2 A. Ben-Naim, *Hydrophobic Interactions*, Plenum Press, New York, 1980.
3 W. Blokzijl and J. B. F. N. Engberts, *Angew. Chem.*, 1993, **105**, 1610–1648.
4 P. L. Privalov and S. J. Gill, *Adv. Protein Chem.*, 1988, **39**, 191–234.
5 N. T. Southall, K. A. Dill and A. D. J. Haymet, *J. Phys. Chem. B*, 2002, **106**, 521–533.
6 L. R. Pratt and A. Pohorille, *Chem. Rev.*, 2002, **102**, 2671–2692.
7 A. Geiger, A. Rahman and F. H. Stillinger, *J. Chem. Phys.*, 1979, **70**, 263–276.
8 C. Pangali, M. Rao and B. J. Berne, *J. Chem. Phys.*, 1979, **71**, 2982–2990.
9 D. A. Zichi and P. J. Rossky, *J. Chem. Phys.*, 1985, **83**, 797–808.
10 D. E. Smith, L. Zhang and A. D. J. Haymet, *J. Am. Chem. Soc.*, 1992, **114**, 5875–5876.
11 D. E. Smith and A. D. J. Haymet, *J. Chem. Phys.*, 1993, **98**, 6445–6454.
12 D. A. Pearlman, *J. Chem. Phys.*, 1993, **98**, 8946–8957.
13 J. Forsman and B. Jönsson, *J. Chem. Phys.*, 1994, **101**, 5116–5125.
14 N. T. Skipper, C. H. Bridgeman, A. D. Buckingham and R. L. Mancera, *Faraday Discuss.*, 1996, **103**, 141–150.
15 S. Lüdemann, H. Schreiber, R. Abseher and O. Steinhauser, *J. Chem. Phys.*, 1996, **104**, 286–295.
16 S. Lüdemann, R. Abseher, H. Schreiber and O. Steinhauser, *J. Am. Chem. Soc.*, 1997, **119**, 4206–4213.
17 V. A. Payne, N. Matubayasi, L. R. Murphy and R. M. Levy, *J. Phys. Chem. B*, 1997, **101**, 2054–2060.
18 T. Ghosh, A. E. García and S. Garde, *J. Am. Chem. Soc.*, 2001, **123**, 1097–1103.
19 T. Ghosh, A. E. García and S. Garde, *J. Chem. Phys.*, 2002, **116**, 2480–2486.
20 T. Ghosh, A. E. García and S. Garde, *J. Phys. Chem. B*, 2003, **107**, 612–617.
21 S. Shimizu and H. S. Chan, *J. Chem. Phys.*, 2000, **113**, 4683–4700.
22 S. Shimizu and H. S. Chan, *J. Am. Chem. Soc.*, 2001, **123**, 2083–2084.
23 S. Shimizu and H. S. Chan, *Proteins: Struct., Funct., Genet.*, 2002, **49**, 560–566.
24 S. W. Rick and B. J. Berne, *J. Phys. Chem. B*, 1997, **101**, 10488–10493.
25 S. W. Rick, *J. Phys. Chem. B*, 2000, **104**, 6884–6888.
26 S. W. Rick, *J. Chem. Phys. B*, 2003, **107**, 9853–9857.
27 D. Paschek, *J. Chem. Phys.*, 2004, **120**, 6674–6690.
28 D. Paschek, *J. Chem. Phys.*, 2004, **120**, 10605–10617.
29 M. S. Moghaddam, S. Shimizu and H. S. Chan, *J. Am. Chem. Soc.*, 2005, **127**, 303–316.
30 E. Wilhelm, R. Battino and R. J. Wilcox, *Chem. Rev.*, 1977, **77**, 219–262.
31 T. R. Rettich, Y. Handa, R. Battino and E. Wilhelm, *J. Phys. Chem.*, 1981, **85**, 3230–3237.
32 H. Naghibi, S. F. Dec and S. J. Gill, *J. Phys. Chem.*, 1986, **90**, 4621–4623.
33 P. L. Privalov, *Crit. Rev. Biochem. Mol. Biol.*, 1990, **25**, 281–305.
34 C. A. Royer, *Biochim. Biophys. Acta*, 2002, **1595**, 201–209.
35 L. Smeller, *Biochim. Biophys. Acta*, 2002, **1595**, 11–29.
36 *Advances in High Pressure Bioscience and Biotechnology*, ed. H. Ludwig, Springer, Heidelberg, Germany, 1999.
37 A. Zipp and W. Kauzmann, *Biochemistry*, 1973, **12**, 4217–4228.
38 S. A. Hawley, *Biochemistry*, 1971, **10**, 2436–2442.
39 J. F. Brandts, R. J. Oliveira and C. Westort, *Biochemistry*, 1970, **9**, 1038–1047.
40 J. L. Silva, D. Foguel and C. A. Royer, *Trends Biochem. Sci.*, 2001, **26**, 612–618.
41 J. L. Silva, C. F. Silveira, A. Correia and L. Pontes, *J. Mol. Biol.*, 1992, **223**, 545–555.
42 X. Peng, J. Jonas and J. L. Silva, *Proc. Natl. Acad. Sci. USA*, 1993, **90**, 1776–1780.
43 G. Panick, G. J. A. Vidugiris, R. Malessa, G. Rapp, R. Winter and C. A. Royer, *Biochemistry*, 1999, **38**, 4157–4164.
44 H. Herberhold and R. Winter, *Biochemistry*, 2002, **41**, 2396–2401.
45 H. Herberhold, C. A. Royer and R. Winter, *Biochemistry*, 2004, **43**, 3336–3345.

46 R. Ravindra, C. Royer and R. Winter, *Phys. Chem. Chem. Phys.*, 2004, **6**, 1952–1961.
47 G. Hummer, S. Garde, A. E. García, M. E. Paulaitis and L. R. Pratt, *Proc. Natl. Acad. Sci. USA*, 1998, **95**, 1552–1555.
48 D. M. Huang and D. Chandler, *Proc. Natl. Acad. Sci. USA*, 2000, **97**, 8324–8327.
49 P. Rein ten Wolde and D. Chandler, *Proc. Natl. Acad. Sci. USA*, 2002, **99**, 6539–6543.
50 D. Chandler, *Nature*, insight review (Preprint), 2005.
51 T. Ghosh, A. Kalra and S. Garde, *J. Phys. Chem. B*, 2005, **109**, 642–651.
52 M. W. Mahoney and W. L. Jorgensen, *J. Chem. Phys.*, 2000, **112**, 8910–8922.
53 S. Nosé, *Mol. Phys.*, 1984, **52**, 255–268.
54 W. G. Hoover, *Phys. Rev. A*, 1985, **31**, 1695–1697.
55 M. Parrinello and A. Rahman, *J. Appl. Phys.*, 1981, **52**, 7180–7182.
56 S. Nosé and M. L. Klein, *Mol. Phys.*, 1983, **50**, 1055–1076.
57 U. Essmann, L. Perera, M. L. Berkowitz, T. A. Darden, H. Lee and L. G. Pedersen, *J. Chem. Phys.*, 1995, **103**, 8577–8593.
58 S. Miyamoto and P. A. Kollman, *J. Comp. Chem.*, 1992, **13**, 952–962.
59 J. P. Ryckaert, G. Ciccotti and H. J. C. Berendsen, *J. Comp. Phys.*, 1977, **23**, 327–341.
60 E. Lindahl, B. Hess and D. van der Spoel, *J. Mol. Model.*, 2001, **7**, 306–317.
61 D. van der Spoel, E. Lindahl, B. Hess, A. R. van Buuren, E. Apol, P. J. Meulenhoff, D. P. Tieleman, A. L. T. M. Sijbers, K. A. Feenstra, R. van Drunen and H. J. C. Berendsen, *Gromacs User Manual version 3.2.*, http://www.gromacs.org, 2004.
62 H. Flyvbjerg and H. G. Petersen, *J. Chem. Phys.*, 1989, **91**, 461–466.
63 H. J. C. Berendsen, J. P. M. Postma, W. F. van Gunsteren, A. DiNola and J. R. Haak, *J. Chem. Phys.*, 1984, **81**, 3684–3690.
64 M. Neumann, *Mol. Phys.*, 1983, **50**, 841–858.
65 J. E. Roberts and J. Schnitker, *J. Chem. Phys.*, 1994, **101**, 5024–5031.
66 J. E. Roberts and J. Schnitker, *J. Phys. Chem.*, 1995, **99**, 1322–1331.
67 W. H. Press, S. A. Teukolsky, W. T. Vetterling and B. P. Flannery, *Numerical Recipes: The Art of Scientific Computing*, Cambridge University Press, Cambridge, 2nd edn., 1992.
68 C. Nicolini, R. Ravindra, B. Ludolph and R. Winter, *Biophys. J.*, 2004, **86**, 1385–1392.
69 V. Daggett and M. Levitt, *Proc. Natl. Acad. Sci. USA*, 1992, **89**, 5142–5146.
70 K. A. T. Silverstein, A. D. J. Haymet and K. A. Dill, *J. Am. Chem. Soc.*, 2000, **122**, 8037–8041.
71 P. De Los Rios and G. Caldarelli, *Phys. Rev. E*, 2000, **62**, 8449–8452.
72 P. De Los Rios and G. Caldarelli, *Phys. Rev. E*, 2001, **63**, 31802.
73 N. Muller, *Acc. Chem. Res.*, 1990, **23**, 23–28.
74 M. I. Marqués, J. M. Borreguerro, H. E. Stanley and N. V. Dokholyan, *Phys. Rev. Lett.*, 2003, **91**, 138103.

